RESEARCH ARTICLE

Synthesis of novel 8 × 8 beam-forming network for broadband multibeam antenna array

Ivan Fanyaev[1] | Ihar Faniayeu[2] (ORCID)

[1]Department of Radiophysics and Electronics, Francisk Skorina Gomel State University, Gomel, Belarus

[2]Department of Physics, University of Gothenburg, Gothenburg, Sweden

Correspondence
Ihar Faniayeu, Department of Physics, University of Gothenburg, 412 96 Gothenburg, Sweden.
Email: ihar.faniayeu@physics.gu.se

Abstract

Synthesis of a novel 8 × 8 beam-forming network (BFN) for broadband multibeam antenna arrays in the X-band has been proposed. The synthesized BFN has 6 less path crossings than a classic Butler matrix. The BFN design is realized using basic elements such as slot-line transition and magic-Ts. A numerical simulation for the analysis of the frequency characteristics of the proposed BFN is carried out. In addition, we offer a design of an eight-channel multibeam antenna array consisting of the synthesized BFN and Vivaldi antennas. Eight spatial beams cover approximately 120° in the azimuth plane with a peak gain of 12 dB in the range of 8.3–11.7 GHz. The proposed broadband multibeam antenna array has good performance, compactness, and ease of fabrication that would be an attractive candidate for radar, satellite communication, and wireless computer networks.

KEYWORDS

beam-forming network, broadband multibeam antenna array, magic-T, synthesis, Vivaldi antenna

1 | INTRODUCTION

New designs of multi-beam antenna arrays have attracted a lot of attention in modern antenna technology to provide highly efficient operation and larger capacity in communication systems. A typical multi-beam antenna array consists of an antenna array, a beam-forming network (BFN) and switches, each part of which has a different function.[1–3] The BFN is the most important part of a multi-beam antenna array system. When the input signal passes through the BFN, an equal-amplitude distribution with a linear phase change is formed at its outputs. The output signal with phase increment would feed the antenna array and depends on the input number. The BFN input port can be defined using switches with multiple independent inputs. As a result, this system can form

multiple beam steering that fully exploits the efficiency of the antenna array while the area of feed network is smaller and more compact than a conventional single-beam antenna.[4–6]

Desirable features of BFN designs are simplicity, compactness, and low dissipation losses with reducing the number of components for easy integration to the antenna system. There are many practical multibeam antenna arrays powering BFNs such as Nolen matrix,[7] Blass Matrix,[8] and Rotman lens,[9] and Butler matrix.[10] The Butler matrix has become the most popular due to its simpler topology that requires the least number of components and low power dissipation (theoretically lossless). The classic Butler matrix allows the generation of N independent beams of $N \times N$ network (N is usually a power of 2) in combination with basic elements such as

couplers, crossovers, and phase shifters.[3,11–14] Application of Butler matrices can be found in direction finding systems,[15] multichannel amplifiers,[16] and multiport measurement systems.[17] Unfortunately, this network has disadvantages with the increase in the number of inputs. For example, the development of classic 8×8 Butler matrices is seldom reported due to their high complexity and a significant number of path crossings in their topology.[18–23] The increase in the number of path crossings leads to large dissipation losses in the BFN. To overcome this problem is usually used the modified Butler matrix having broadside beam, endfire beam, and intermediate beams distributed evenly.[24–27] The inputs and outputs of such modified Butler matrix are located on all sides of BFN that leads to technical difficulties in feeding with the antenna array. Therefore, it is necessary to find a new approach for the realization of BFNs with a minimum number of path crossings and a simple connection with the antenna array.

In this article, we synthesized and designed a novel 8×8 BFN for the broadband multibeam antenna array in the X-band. The analytically synthesized BFN has 6 less path crossings than the classic Butler matrix. The implementation of the BFN in the form of a three-layer printed circuit board (PCB) using broadband slot-line transition and magic tees (magic-Ts) is proposed. The designed BFN is constructively simply connected to the eight-channel Vivaldi antenna array. The characterization was performed with numerical simulation for separate synthesized BFN and with Vivaldi antenna array in the X-band.

2 | SYNTHESIS OF NOVEL BEAM-FORMING NETWORKS

We aim to synthesize a new orthogonal BFN with less number path crossings than in the traditional Butler matrix. That allows us to simplify the BFN topology and decrease dissipation losses. The construction of BFNs involves the determination of their structure, the composition of basic elements and requirements to their denominations on the basis of predetermined system parameters. There are different approaches for the synthesis of BFNs with an arbitrary number of inputs and outputs.[28,29] However, the proposed methods include a large number of path crossings in synthesized networks. We are interested in another approach to the synthesis of BFNs with an arbitrary number of inputs based on the scattering matrix.[30] The advantage of this method is the arbitrary choice of actions in the construction of the BFNs, which gives a certain freedom in the choice of the specified parameters to achieve the final goal, for example, to reduce the number of path crossings or phase shifters. Here, we adopt this approach to synthesis a new 8×8 BFN with less number of path crossings based on a specified scattering matrix with the required amplitude-phase distribution.

To synthesize the new BFN, we utilize a scattering matrix with the described amplitude-phase distribution at the outputs as follows:

$$S_{\text{BFN}} = \begin{bmatrix} O & S^T \\ S & O \end{bmatrix} \quad (1)$$

where O is an 8×8 null matrix describing the mutual isolation and matching of inputs, S is a scattering matrix describing the distribution of signals in the output transmission lines of the distribution multipole. The given scattering matrix with a definite phase distribution has the form:

$$S_{m,n} = \frac{1}{\sqrt{N}} e^{-j\varphi_{m,n}} \quad (2)$$

$$\varphi_{m,n} = \begin{bmatrix} 202.5° & 202.5° & 225° & 270° & 112.5° & 112.5° & 135° & 180° \\ 45° & 90° & 157.5° & 247.5° & 135° & 180° & 247.5° & 337.5° \\ 247.5° & 337.5° & 90° & 225° & 157.5° & 247.5° & 0° & 135° \\ 90° & 225° & 22.5° & 202.5° & 180° & 315° & 112.5° & 292.5° \\ 292.5° & 112.5° & 315° & 180° & 202.5° & 22.5° & 225° & 90° \\ 135° & 0° & 247.5° & 157.5° & 225° & 90° & 337.5° & 247.5° \\ 337.5° & 247.5° & 180° & 135° & 247.5° & 157.5° & 90° & 45° \\ 180° & 135° & 112.5° & 112.5° & 270° & 225° & 202.5° & 202.5° \end{bmatrix} \quad (3)$$

where $N = 8$ is the number of outputs with output number m and input number n.

The network of a nondissipative distribution multipole with a given scattering matrix (1) is composed in the form of a cascade connection of the simplest distribution multipoles of the same dimension. Each cascade must be simple so that its structure can be recreated using its scattering matrix and the denominations of the elements can be determined. This requirement is satisfied by distribution multipoles, which have an elementary unitary matrix as the scattering matrix, which differs from the identity matrix E only by four elements α, β, γ, δ, forming a unitary matrix of the second order as follows:

$$
T_M = \begin{array}{c} \\ 1 \\ 2 \\ k \\ \vdots \\ l \\ \vdots \\ N \end{array}
\begin{array}{cc}
\begin{array}{cccccc} 1 & 2 & k & \cdots & l & \cdots & N \end{array} \\
\left[\begin{array}{ccccccc}
1 & 0 & \vdots & & \vdots & & 0 \\
0 & 1 & \vdots & & \vdots & & 0 \\
\cdots & \cdots & \alpha & \cdots & \gamma & \cdots & \cdots \\
& & \vdots & & \vdots & & \\
\cdots & \cdots & \beta & \cdots & \delta & \cdots & \cdots \\
& & \vdots & & \vdots & & \\
0 & 0 & \vdots & & \vdots & & 1
\end{array}\right]
\end{array} \quad (4)
$$

where T_M is multiplier-matrix of the elementary cascade of the distribution multipole, M is number of the cascade, (k, l) are matrix cell numbers. Parameters α, β, γ, δ can be obtain from following formulas:[30]

$$
|\alpha| = |\delta| = \frac{|S_{m,k}|}{\sqrt{|S_{m,k}|^2 + |S_{m,l}|^2}} \quad (5a)
$$

$$
|\beta| = |\gamma| = \sqrt{1 - |\alpha|^2} \quad (5b)
$$

$$
\arg(\alpha) - \arg(\beta) = \arg(S_{m,l}) - \arg(S_{m,k}) \quad (5c)
$$

$$
\arg(\gamma) - \arg(\delta) = \mp\pi + \arg(\alpha) - \arg(\beta) \quad (5d)
$$

with the arbitrary phase of parameters α, β, γ, δ.

The next multiplier-matrix T_{M-1}, corresponding to the penultimate cascade of the distribution multipole, is selected so that another zero element is formed in the first row. The procedure continues until, for example, only one element is nonzero in the first row. Parameters of the last multiplier-matrix T_{M-N+2} are determined from the relations:

$$
\alpha = S'_{m,k}, \beta = S'_{m,l}, \; |\alpha| = |\delta|, \; |\beta| = |\gamma| \quad (6a)
$$

$$
\arg(\gamma) - \arg(\delta) = \mp\pi + \arg(\alpha) - \arg(\beta) \quad (6b)
$$

where $S'_{m,k}$ and $S'_{m,l}$ the elements of the matrix obtained before multiplying by T_{M-N+2}.

The matrix S is a unitary matrix of $S^{-1} \cdot S = E$ due to the absence of dissipation of an ideal distribution multipole. Therefore, we take the inverse matrix of S as $S^{-1} = T_t^*$. Let us choose the first of the elementary matrices T_M realizing the renumbering of outputs in the form of segments of transmission lines of zero length, which corresponds to the last cascade of the multipole:

$$
T_M = \begin{bmatrix}
1 & 0 & 0 & 0 & 0 & 0 & 0 & 0 \\
0 & 0 & 1 & 0 & 0 & 0 & 0 & 0 \\
0 & 0 & 0 & 0 & 1 & 0 & 0 & 0 \\
0 & 0 & 0 & 0 & 0 & 0 & 1 & 0 \\
0 & 1 & 0 & 0 & 0 & 0 & 0 & 0 \\
0 & 0 & 0 & 1 & 0 & 0 & 0 & 0 \\
0 & 0 & 0 & 0 & 0 & 1 & 0 & 0 \\
0 & 0 & 0 & 0 & 0 & 0 & 0 & 1
\end{bmatrix}. \quad (7)
$$

As a result, we obtain the following matrix:

$$
T_t^* \cdot T_M = \frac{1}{\sqrt{8}} e^{-j\varphi^1} \quad (8)
$$

$$
\varphi^1 = \begin{bmatrix}
157.5° & 67.5° & 315° & 225° & 112.5° & 22.5° & 270° & 180° \\
157.5° & 247.5° & 270° & 0° & 22.5° & 112.5° & 135° & 225° \\
135° & 45° & 202.5° & 112.5° & 270° & 180° & 337.5° & 247.5° \\
90° & 180° & 112.5° & 202.5° & 135° & 225° & 157.5° & 247.5° \\
247.5° & 157.5° & 225° & 135° & 202.5° & 112.5° & 180° & 90° \\
247.5° & 337.5° & 180° & 270° & 112.5° & 202.5° & 45° & 135° \\
225° & 135° & 112.5° & 22.5° & 0° & 270° & 247.5° & 157.5° \\
180° & 270° & 22.5° & 112.5° & 225° & 315° & 67.5° & 157.5°
\end{bmatrix}. \quad (9)
$$

Next, we choose the second of the elementary unitary matrices T_{M-1} with parameters α, β, γ, δ in the first and second columns and calculate so that the second element of the first row vanishes. Substituting into the formulas (5a)–(5d) of $S_{n,k} = \frac{1}{\sqrt{8}} e^{-j157.5°}$ and $S_{n,m} = \frac{1}{\sqrt{8}} e^{-j67.5°}$, we find that $|\alpha| = |\delta| = |\beta| = |\gamma| = \frac{1}{\sqrt{2}}$, $\arg(\alpha) - \arg(\beta) = 90°$, $\arg(\gamma) - \arg(\delta) = -90°$. Assume for the definition that

$\arg(\alpha) = \arg(\delta) = 0$, we obtain T_{M-1} matrix in the following form:

$$T_{M-1} = \frac{1}{\sqrt{2}} \begin{bmatrix} e^{-j0°} & e^{-j90°} & 0 & 0 & 0 & 0 & 0 & 0 \\ e^{-j90°} & e^{-j0°} & 0 & 0 & 0 & 0 & 0 & 0 \\ 0 & 0 & \sqrt{2} & 0 & 0 & 0 & 0 & 0 \\ 0 & 0 & 0 & \sqrt{2} & 0 & 0 & 0 & 0 \\ 0 & 0 & 0 & 0 & \sqrt{2} & 0 & 0 & 0 \\ 0 & 0 & 0 & 0 & 0 & \sqrt{2} & 0 & 0 \\ 0 & 0 & 0 & 0 & 0 & 0 & \sqrt{2} & 0 \\ 0 & 0 & 0 & 0 & 0 & 0 & 0 & \sqrt{2} \end{bmatrix} \tag{10}$$

Such matrix corresponds to the elements of a directional coupler between the first and second inputs and outputs while the remaining inputs are connected directly to the outputs. A multiplier-matrix with a directional coupler can be written in the compact form as

$$T_{M-1} = \frac{1}{\sqrt{2}} \cdot \begin{matrix} & 1 & 2 \\ 1 \\ 2 \end{matrix} \begin{bmatrix} e^{-j0°} & e^{-j90°} \\ e^{-j90°} & e^{-j0°} \end{bmatrix} \tag{11}$$

The numbers above and on the side indicate the cell numbers (k, l) of matrix with parameters α, β, γ, δ. All off-diagonal elements are zero, and the remaining diagonal elements are equal to one.

The third elementary unitary matrix T_{M-2} is calculated so that the fourth element of the first row in the third and fourth columns vanishes. Parameters α, β, γ, δ

turn out to be similar to the previous ones, and the matrix T_{M-2} can be written as:

$$T_{M-2} = \frac{1}{\sqrt{2}} \cdot \begin{matrix} & 3 & 4 \\ 3 \\ 4 \end{matrix} \begin{bmatrix} e^{-j0°} & e^{-j90°} \\ e^{-j90°} & e^{-j0°} \end{bmatrix}. \tag{12}$$

Further, we turn to zero the sixth and eighth element of the first row:

$$T_{M-3} = \frac{1}{\sqrt{2}} \cdot \begin{matrix} & 5 & 6 \\ 5 \\ 6 \end{matrix} \begin{bmatrix} e^{-j0°} & e^{-j90°} \\ e^{-j90°} & e^{-j0°} \end{bmatrix} \tag{13}$$

$$T_{M-4} = \frac{1}{\sqrt{2}} \cdot \begin{matrix} & 7 & 8 \\ 7 \\ 8 \end{matrix} \begin{bmatrix} e^{-j0°} & e^{-j90°} \\ e^{-j90°} & e^{-j0°} \end{bmatrix}. \tag{14}$$

The next elementary matrix T_{M-5} implements renumbering of outputs as follows:

$$T_{M-5} = \begin{bmatrix} 1 & 0 & 0 & 0 & 0 & 0 & 0 & 0 \\ 0 & 0 & 0 & 0 & 1 & 0 & 0 & 0 \\ 0 & 1 & 0 & 0 & 0 & 0 & 0 & 0 \\ 0 & 0 & 0 & 0 & 0 & 1 & 0 & 0 \\ 0 & 0 & 1 & 0 & 0 & 0 & 0 & 0 \\ 0 & 0 & 0 & 0 & 0 & 0 & 1 & 0 \\ 0 & 0 & 0 & 1 & 0 & 0 & 0 & 0 \\ 0 & 0 & 0 & 0 & 0 & 0 & 0 & 1 \end{bmatrix}. \tag{15}$$

$$T_t^* \cdot T_M \cdot T_{M-1} \cdot T_{M-2} \cdot T_{M-3} \cdot T_{M-4} \cdot T_{M-5}$$

$$= \frac{1}{2} \begin{bmatrix} e^{-j157.5°} & e^{-j315°} & e^{-j112.5°} & e^{-j270°} & 0 & 0 & 0 & 0 \\ 0 & 0 & 0 & 0 & e^{-j247.5°} & e^{-j0°} & e^{-j112.5°} & e^{-j225°} \\ e^{-j135°} & e^{-j202.5°} & e^{-j270°} & e^{-j337.5°} & 0 & 0 & 0 & 0 \\ 0 & 0 & 0 & 0 & e^{-j180°} & e^{-j202.5°} & e^{-j225°} & e^{-j247.5°} \\ e^{-j247.5°} & e^{-j225°} & e^{-j202.5°} & e^{-j180°} & 0 & 0 & 0 & 0 \\ 0 & 0 & 0 & 0 & e^{-j337.5°} & e^{-j270°} & e^{-j202.5°} & e^{-j135°} \\ e^{-j225°} & e^{-j112.5°} & e^{-j0°} & e^{-j247.5°} & 0 & 0 & 0 & 0 \\ 0 & 0 & 0 & 0 & e^{-j270°} & e^{-j112.5°} & e^{-j315°} & e^{-j157.5°} \end{bmatrix}. \tag{16}$$

As a result of the multiplying of all elementary matrices, we obtain:

Next, we choose the seventh elementary unitary matrices T_{M-6} with parameters α, β, γ, δ in the first and second columns and calculate so that the second element of the first row vanishes:

$$T_{M-6} = \frac{1}{\sqrt{2}} \cdot \begin{array}{c} \\ 1 \\ 2 \end{array} \overset{\begin{array}{cc} 1 & 2 \end{array}}{\begin{bmatrix} e^{-j0°} & e^{-j337.5°} \\ e^{-j202.5°} & e^{-j0°} \end{bmatrix}}. \tag{17}$$

Eighth elementary unitary matrix T_{M-7} is obtained by vanishing the fourth element of the first row as

$$T_{M-7} = \frac{1}{\sqrt{2}} \cdot \begin{array}{c} \\ 3 \\ 4 \end{array} \overset{\begin{array}{cc} 3 & 4 \end{array}}{\begin{bmatrix} e^{-j0°} & e^{-j337.5°} \\ e^{-j202.5°} & e^{-j0°} \end{bmatrix}}. \tag{18}$$

Similarly, matrices T_{M-8} and T_{M-9} are obtained by the vanishing of the sixth and eighth elements of the second row:

$$T_{M-9} = \frac{1}{\sqrt{2}} \cdot \begin{array}{c} \\ 7 \\ 8 \end{array} \overset{\begin{array}{cc} 7 & 8 \end{array}}{\begin{bmatrix} e^{-j0°} & e^{-j292.5°} \\ e^{-j247.5°} & e^{-j0°} \end{bmatrix}}. \tag{20}$$

Next, the matrix T_{M-10} implements renumbering of outputs in the following way:

$$T_{M-10} = \begin{bmatrix} 1 & 0 & 0 & 0 & 0 & 0 & 0 & 0 \\ 0 & 0 & 1 & 0 & 0 & 0 & 0 & 0 \\ 0 & 1 & 0 & 0 & 0 & 0 & 0 & 0 \\ 0 & 0 & 0 & 1 & 0 & 0 & 0 & 0 \\ 0 & 0 & 0 & 0 & 1 & 0 & 0 & 0 \\ 0 & 0 & 0 & 0 & 0 & 0 & 1 & 0 \\ 0 & 0 & 0 & 0 & 0 & 1 & 0 & 0 \\ 0 & 0 & 0 & 0 & 0 & 0 & 0 & 1 \end{bmatrix}. \tag{21}$$

By multiplying all obtained elementary matrices, we can write as

In the first row of this matrix, only one second element remains to zero. Therefore, to deter-

$$T_t^* \cdot T_M \cdot T_{M-1} \cdot T_{M-2} \cdot T_{M-3} \cdot T_{M-4} \cdot T_{M-5} \cdot T_{M-6} \cdot T_{M-7} \cdot T_{M-8} \cdot T_{M-9} \cdot T_{M-10}$$

$$= \begin{bmatrix} \frac{e^{-j157.5°}}{\sqrt{2}} & \frac{e^{-j112.5°}}{\sqrt{2}} & 0 & 0 & 0 & 0 & 0 & 0 \\ 0 & 0 & 0 & 0 & \frac{e^{-j247.5°}}{\sqrt{2}} & \frac{e^{-j112.5°}}{\sqrt{2}} & 0 & 0 \\ \frac{e^{-j90°}}{2} & \frac{e^{-j225°}}{2} & \frac{e^{-j157.5°}}{2} & \frac{e^{-j292.5°}}{2} & 0 & 0 & 0 & 0 \\ 0 & 0 & 0 & 0 & \frac{e^{-j135°}}{2} & \frac{e^{-j135°}}{2} & \frac{e^{-j157.5°}}{2} & \frac{e^{-j202.5°}}{2} \\ 0 & 0 & \frac{e^{-j225°}}{\sqrt{2}} & \frac{e^{-j180°}}{\sqrt{2}} & 0 & 0 & 0 & 0 \\ 0 & 0 & 0 & 0 & 0 & 0 & \frac{e^{-j270°}}{\sqrt{2}} & \frac{e^{-j135°}}{\sqrt{2}} \\ \frac{e^{-j270°}}{2} & \frac{e^{-j45°}}{2} & \frac{e^{-j157.5°}}{2} & \frac{e^{-j292.5°}}{2} & 0 & 0 & 0 & 0 \\ 0 & 0 & 0 & 0 & \frac{e^{-j315°}}{2} & \frac{e^{-j0°}}{2} & \frac{e^{-j157.5°}}{2} & \frac{e^{-j202.5°}}{2} \end{bmatrix}. \tag{22}$$

$$T_{M-8} = \frac{1}{\sqrt{2}} \cdot \begin{array}{c} \\ 5 \\ 6 \end{array} \overset{\begin{array}{cc} 5 & 6 \end{array}}{\begin{bmatrix} e^{-j0°} & e^{-j292.5°} \\ e^{-j247.5°} & e^{-j0°} \end{bmatrix}}. \tag{19}$$

mine the next elementary unitary matrix T_{M-11} it is necessary to use formulas (6a) and (6b). Substituting in these formulas $S_{1,1} = \frac{1}{\sqrt{2}} e^{-j157.5°}$ and $S_{1,2} = \frac{1}{\sqrt{2}} e^{-j112.5°}$, we can find necessary parameters as follows:
$|\alpha| = \frac{1}{\sqrt{2}} e^{-j202.5°}$, $\qquad |\beta| = \frac{1}{\sqrt{2}} e^{-j247.5°}$, $\qquad |\delta| = |\gamma| = \frac{1}{\sqrt{2}}$,

$\arg(\gamma) - \arg(\delta) = \pi + 202.5° - 247.5°$. Suppose for the definition that $\arg(\gamma) = 0$, we obtain a matrix T_{M-11} in the following form:

$$T_t^* \cdot T_M \cdot T_{M-1} \cdot T_{M-2} \cdot T_{M-3} \cdot T_{M-4} \cdot T_{M-5} \cdot T_{M-6} \cdot T_{M-7} \cdot T_{M-8} \cdot T_{M-9} \cdot T_{M-10} \cdot T_{M-11} \cdot T_{M-12} \cdot T_{M-13} \cdot T_{M-14}$$

$$= \frac{1}{\sqrt{2}} \begin{bmatrix} \sqrt{2} & 0 & 0 & 0 & 0 & 0 & 0 & 0 \\ 0 & 0 & 0 & 0 & \sqrt{2} & 0 & 0 & 0 \\ 0 & e^{-j90°} & e^{-j157.5°} & 0 & 0 & 0 & 0 & 0 \\ 0 & 0 & 0 & 0 & 0 & e^{-j135°} & e^{-j157.5°} & 0 \\ 0 & 0 & 0 & \sqrt{2} & 0 & 0 & 0 & 0 \\ 0 & 0 & 0 & 0 & 0 & 0 & 0 & \sqrt{2} \\ 0 & e^{-j270°} & e^{-j157.5°} & 0 & 0 & 0 & 0 & 0 \\ 0 & 0 & 0 & 0 & 0 & e^{-j315°} & e^{-j157.5°} & 0 \end{bmatrix}. \tag{27}$$

$$T_{M-11} = \frac{1}{\sqrt{2}} \cdot \begin{array}{c} \\ 1 \\ 2 \end{array} \overset{\begin{array}{cc} 1 & 2 \end{array}}{\begin{bmatrix} e^{-j157.5°} & e^{-j0°} \\ e^{-j247.5°} & e^{-j225°} \end{bmatrix}}. \tag{23}$$

Similar to the previous steps, the matrix T_{M-12} is obtained by vanishing the fourth element of the third row:

$$T_{M-12} = \frac{1}{\sqrt{2}} \cdot \begin{array}{c} \\ 3 \\ 4 \end{array} \overset{\begin{array}{cc} 3 & 4 \end{array}}{\begin{bmatrix} e^{-j0°} & e^{-j315°} \\ e^{-j225°} & e^{-j0°} \end{bmatrix}}. \tag{24}$$

In the second row, there is only a single sixth element left to zero. Using formulas (6a) and (6b), we obtain matrices T_{M-13} and T_{M-14} in the following form:

$$T_{M-13} = \frac{1}{\sqrt{2}} \cdot \begin{array}{c} \\ 5 \\ 6 \end{array} \overset{\begin{array}{cc} 5 & 6 \end{array}}{\begin{bmatrix} e^{-j112.5°} & e^{-j0°} \\ e^{-j247.5°} & e^{-j315°} \end{bmatrix}} \tag{25}$$

$$T_{M-14} = \frac{1}{\sqrt{2}} \cdot \begin{array}{c} \\ 7 \\ 8 \end{array} \overset{\begin{array}{cc} 7 & 8 \end{array}}{\begin{bmatrix} e^{-j0°} & e^{-j225°} \\ e^{-j315°} & e^{-j0°} \end{bmatrix}}. \tag{26}$$

By multiplying all obtained matrices we can write them as

Next, only one third element needs to convert to zero in the third row and the seventh element in the fourth row. These matrices T_{M-15} and T_{M-16} have the following form:

$$T_{M-15} = \frac{1}{\sqrt{2}} \cdot \begin{array}{c} \\ 2 \\ 3 \end{array} \overset{\begin{array}{cc} 2 & 3 \end{array}}{\begin{bmatrix} e^{-j270°} & e^{-j0°} \\ e^{-j202.5°} & e^{-j112.5°} \end{bmatrix}} \tag{28}$$

$$T_{M-16} = \frac{1}{\sqrt{2}} \cdot \begin{array}{c} \\ 6 \\ 7 \end{array} \overset{\begin{array}{cc} 6 & 7 \end{array}}{\begin{bmatrix} e^{-j225°} & e^{-j0°} \\ e^{-j202.5°} & e^{-j157.5°} \end{bmatrix}}. \tag{29}$$

It remains only to extract the penultimate matrix T_{M-17} by renumbering outputs as follows:

$$T_{M-17} = \begin{bmatrix} 1 & 0 & 0 & 0 & 0 & 0 & 0 & 0 \\ 0 & 0 & 1 & 0 & 0 & 0 & 0 & 0 \\ 0 & 0 & 0 & 0 & 0 & 0 & 1 & 0 \\ 0 & 0 & 0 & 0 & 1 & 0 & 0 & 0 \\ 0 & 1 & 0 & 0 & 0 & 0 & 0 & 0 \\ 0 & 0 & 0 & 1 & 0 & 0 & 0 & 0 \\ 0 & 0 & 0 & 0 & 0 & 0 & 0 & 1 \\ 0 & 0 & 0 & 0 & 0 & 1 & 0 & 0 \end{bmatrix}. \tag{30}$$

The last multiplier-matrix T_{M-18} corresponds to the first cascade of the network and defines as the inverse matrix obtained by the multiplication of all elementary matrices as
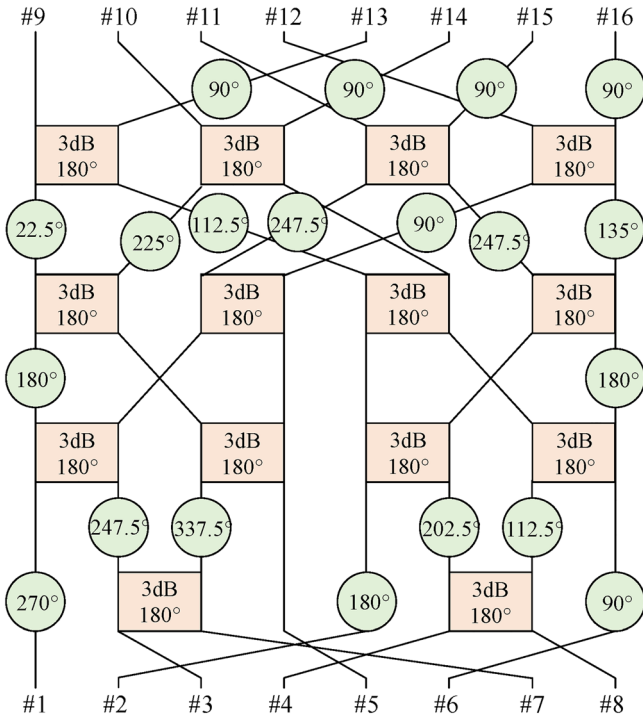
FIGURE 1 Topology of the synthesized 8×8 beam-forming network

$$T_{M-18} = \begin{bmatrix} 1 & 0 & 0 & 0 & 0 & 0 & 0 & 0 \\ 0 & 1 & 0 & 0 & 0 & 0 & 0 & 0 \\ 0 & 0 & 1 & 0 & 0 & 0 & 0 & 0 \\ 0 & 0 & 0 & 1 & 0 & 0 & 0 & 0 \\ 0 & 0 & 0 & 0 & e^{-j180°} & 0 & 0 & 0 \\ 0 & 0 & 0 & 0 & 0 & e^{-j225°} & 0 & 0 \\ 0 & 0 & 0 & 0 & 0 & 0 & e^{-j90°} & 0 \\ 0 & 0 & 0 & 0 & 0 & 0 & 0 & e^{-j45°} \end{bmatrix}. \quad (31)$$

The matrix T_{M-18} describes a set of different phase shifters that are connected to the corresponding outputs. The end result of the multiplication of all elementary matrices must be the identity matrix E. Combining all 19 elementary cascades, we obtain the new BFN with 8×8 outputs.

We choose a directional coupler in the form of Magic-Ts with a scattering matrix as

$$S_T = \frac{1}{\sqrt{2}} \begin{bmatrix} 0 & 0 & e^{-j270°} & e^{-j270°} \\ 0 & 0 & e^{-j90°} & e^{-j270°} \\ e^{-j270°} & e^{-j90°} & 0 & 0 \\ e^{-j270°} & e^{-j270°} & 0 & 0 \end{bmatrix}. \quad (32)$$

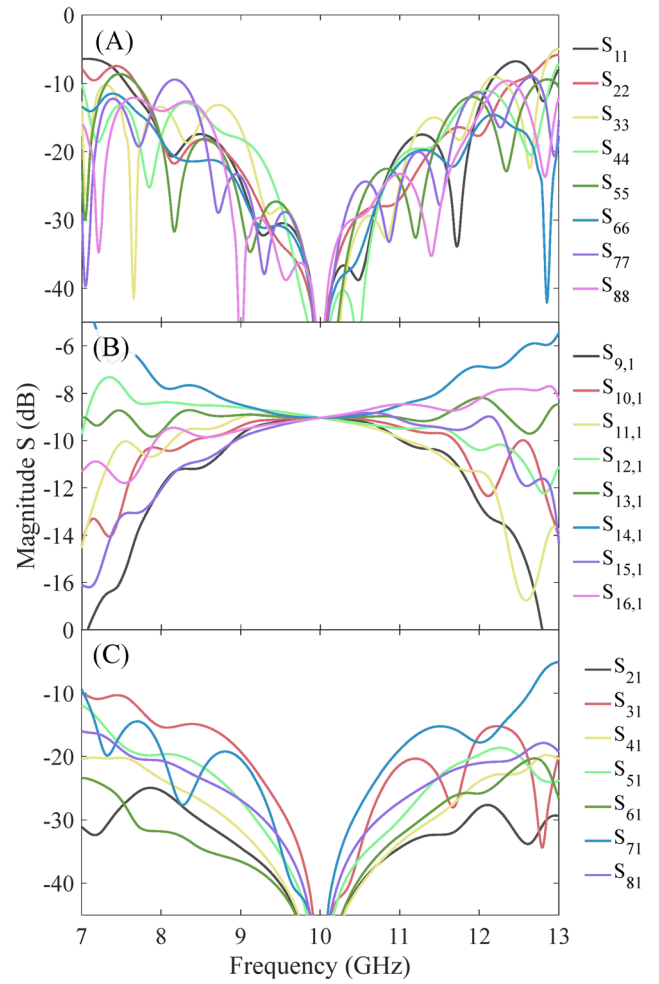We achieved the final topology of the new BFN after selecting the phase shifts at the inputs and outputs of

FIGURE 2 Analytically calculated S-parameters of the synthesized BFN. (A) reflection coefficients of inputs #1 to #8, (B) transmission coefficients when port #1 is fed, and (C) isolations input port #1

each magic-Ts in accordance with its multiplier-matrix depicted in Figure 1. The squares represent 3 dB directional couplers with 180° phase shifts and circles indicate phase shifters. The numbers at the bottom and top mean the inputs and outputs of the BFN. Figure 1 shows that the synthesized BFN has 14 path crossings if we exclude the sequential numbering of the inputs. The total number of path crossings is 22 which is 6 less than in the classical Butler matrix. The synthesized BFN has a symmetric topology similar to the Butler matrix.

Here, we analytically calculate the synthesized BFN (Figure 1) using the described approach above and the method of decomposition of symmetric eight-port networks (method of in-phase and opposite-phase excitation) as well as the cascade connection of two networks with known scattering matrices.[30] The main characteristics of the synthesized BFN of 8×8 outputs in the frequency range were analytically calculated in the range of 7–13 GHz.
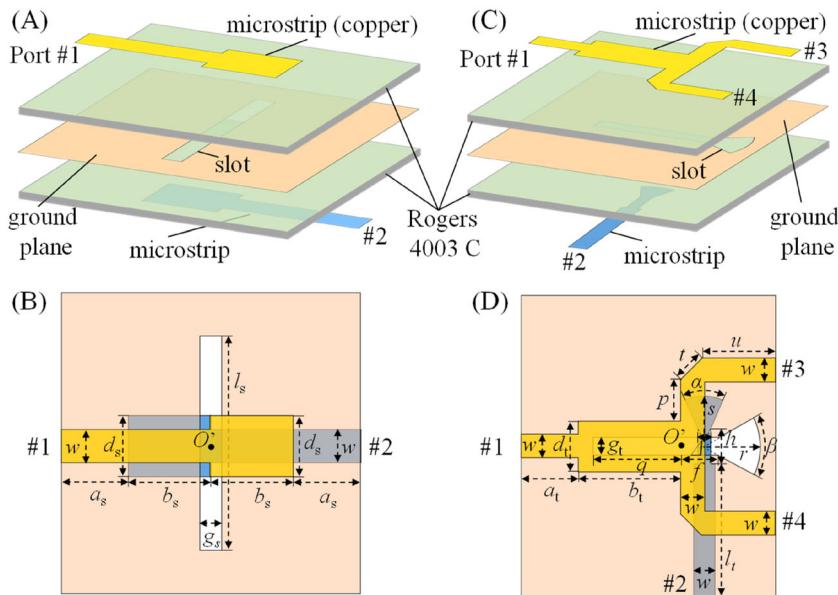
FIGURE 3 The design of the basic elements. Slot-line transition: (A) General view of the proposed slot-line transition and (B) top view without dielectric Rogers with defined structural parameters; (C) perspective view of the magic-T and its (D) top view with structural parameters

TABLE 1 Geometric parameters of slot-line transition and magic-T which are depicted in Figure 1B,D. Given lengths are in mm

Parameters	Value	Parameters	Value
w	1.14	q	4.2
d_s	2.1	f	1.4
a_s	2.9	s	2.5
b_s	2.35	r	2.5
g_s	0.8	h	1.85
l_s	7.5	p	1.88
d_t	2.35	t	1.47
a_t	2.65	u	3.3
b_t	4.75	Δ	0.8
g_t	0.8	α	50°
l_t	7.05	β	60°

FIGURE 4 Simulated S-parameters of (A) slot-line transition and (B) magic-T. S_{11}, S_{22}, S_{33}, and S_{44} coefficients mean return losses at ports; S_{34} is port-to-port isolation; S_{31} is in-phase transmission; S_{32} and S_{42} are out-of-phase transmission coefficients, respectively

Figure 2 shows the analytically calculated main characteristics of BFN: the reflection coefficients at all inputs (Figure 2A), the transmission coefficients from the first input to the BFN outputs (Figure 2B), and the coupling coefficients of the first input (Figure 2C). It is seen from calculated results that the reflection coefficients are below −15 dB in the frequency range 8.5–11.5 GHz. In the analytical calculation of BFN, losses were not taken into account, therefore, the transfer coefficients from input #1 to outputs #9–16 are in the range from −8 to −11 dB within the operating bandwidth. According to Figure 2C, the isolation of input port #1 is −15 dB. Further, it can be seen that analytically calculated results (Figure 2) and numerically simulated results (Figure 6) are in good agreement that confirm the performance of the synthesized BFN.
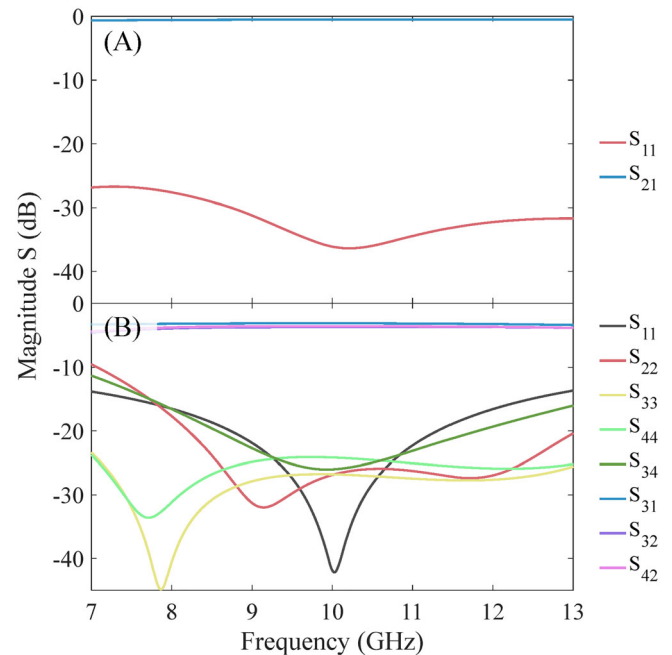
3 | MULTIBEAM ANTENNA ARRAY

3.1 | Basic elements analysis

An important feature in the construction of the BFN topology is the choice of basic elements, their compact placement on the board, as well as the implementation of
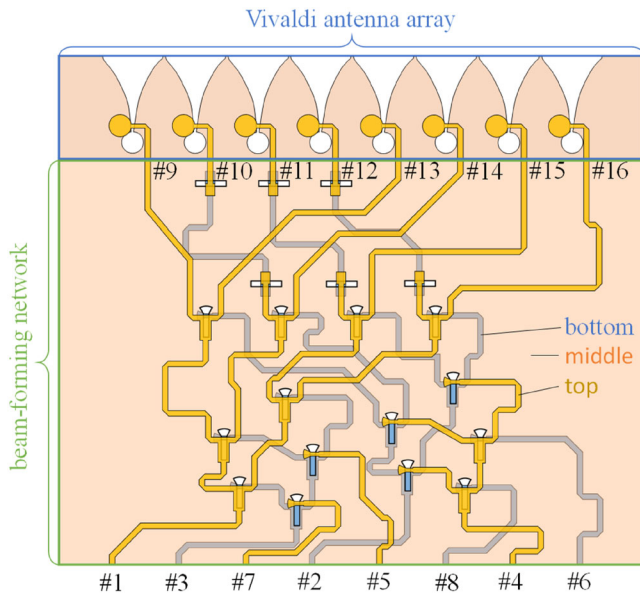
FIGURE 5 The design of the synthesized 8 × 8 BFN connected with Vivaldi antenna array for broadband and wide-angle multibeam steering

FIGURE 6 S-parameters of proposed BFN. (A) reflection coefficients of inputs #1 to #8, (B) transmission coefficients when port #1 is fed, and (C) isolations input port #1

the network without path crossings. We propose to design the BFN based on broadband slot-line transition and magic-Ts as basic elements. The slot-line transition elements are characterized by bandwidths from an octave[31] up to one decade in the 1–10 GHz range.[32] In our case, we modified and optimized by numerical simulation the slot-line transition element for X-band described in articles.[33,34] The traditional magic-Ts are four-port multipole that provide in-phase and out-of-phase signal division between their two output ports.[35–37] They are similar to many different planar basic elements such as branch-line, rat-race, or directional couplers.[38] Here we use one of the designs described in reference.[39] Using these elements, it is possible to design a compact topology of the proposed 8 × 8 BFN on a three-layer printed circuit board.

The slot-line transition element for X-band is shown in Figure 3A,B. Its conductors are located relative to a narrow slot resonator with a length of $\lambda_0/4$ (λ_0 is the wavelength at the central frequency of the operation band) mirrored to each other and matched by rectangular microstrips (plugs). A Rogers 4003 C dielectric with a dielectric constant of 3.38 and a loss tangent of 0.0027 was used as a substrate. We use a standard thickness of the dielectric substrate of 0.508 mm and a copper layer (microstrip) of 35 μm. The design of the proposed magic-T is shown in Figure 3C,D. There is no capacitive cutout between outputs #3 and #4 in this magic-T topology. A narrow resonance slot at one end is made in the form of a radial plug. Input #2 is matched with a transition to higher resistance and a radial plug on the end.
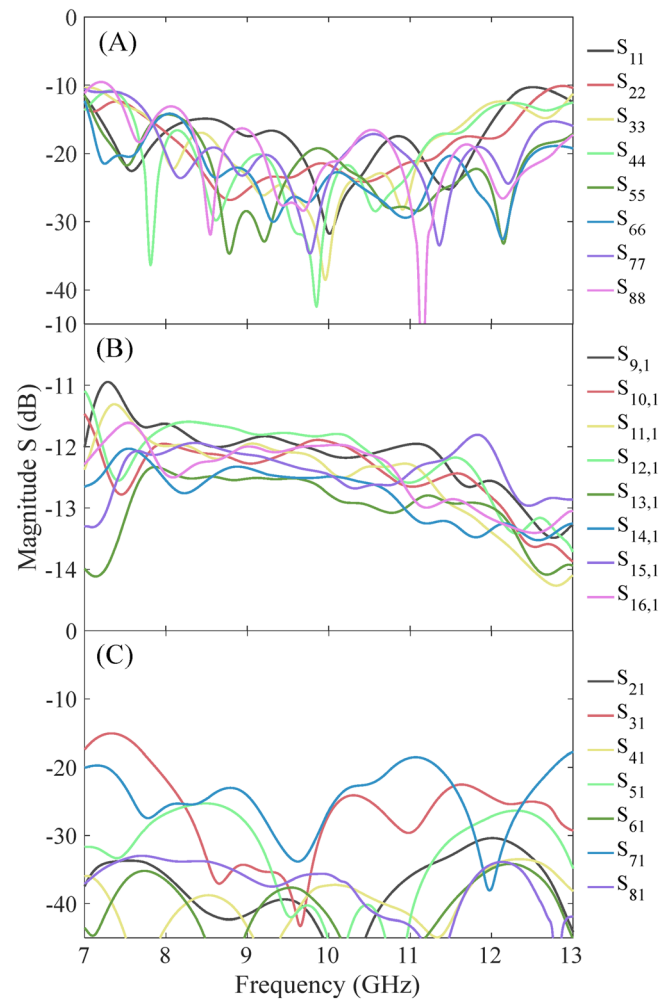
The structural parameters of the slot-line transition element and the magic-T shown in Figure 3B,D are given in Table 1.

The characterization of the proposed basic elements of BFN was carried out using numerical electromagnetic simulation based on the finite element method. Figure 4 shows the S-parameters of the slot-line transition and the magic-T in the frequency range of 7–13 GHz. As seen from Figure 4A, the reflection coefficient does not exceed −28 dB in the entire frequency range which is 2 dB lower in comparison with reference.[39] The slot-line transition element carries out only the transition of electromagnetic energy from one side of the board to the other, therefore, the transmission coefficient has an average value of −0.55 ± 0.04 dB in the entire X-band. The basic element does not introduce a phase shift at a central frequency of 10 GHz ($\lambda_0 = 30$ mm) with the phase of 0.5°. The maximum phase imbalance is less than 4° in the operating frequency range.
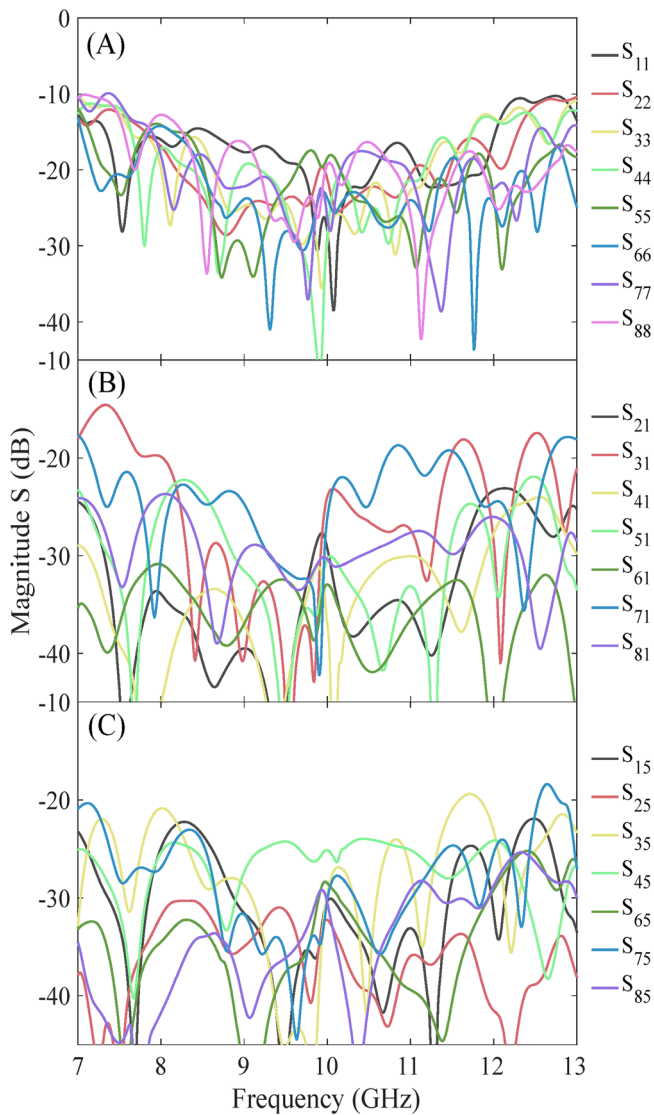
FIGURE 7 *S*-parameters of antenna array. (A) reflection coefficients of inputs #1–#8. (B) Isolations input port #1 and (C) input port #5

FIGURE 8 The radiation pattern of the proposed eight-beam antenna array in the azimuth plane at (A) 8.3 GHz, (B) 10 GHz, and (C) 11.7 GHz, respectively

The simulated results show that within the frequency range from 8 to 12 GHz for magic-T (Figure 4B) the insertion losses $S_{31(41)}$ for in-phase and $S_{32(42)}$ for out-of-phase excitation are less than -3.5 ± 0.4 dB, while the return losses for ports #1 and #2 are more than -16 dB and -18 dB, respectively. The isolations S_{34} and S_{21} are greater than -16 dB and -40 dB, respectively.

3.2 | Analysis of the synthesized BFN

The three-layer PCB design of a novel 8×8 BFN based on proposed slot-line transitions and magic-Ts for broadband multibeam antenna array is illustrated in Figure 5. The basic elements a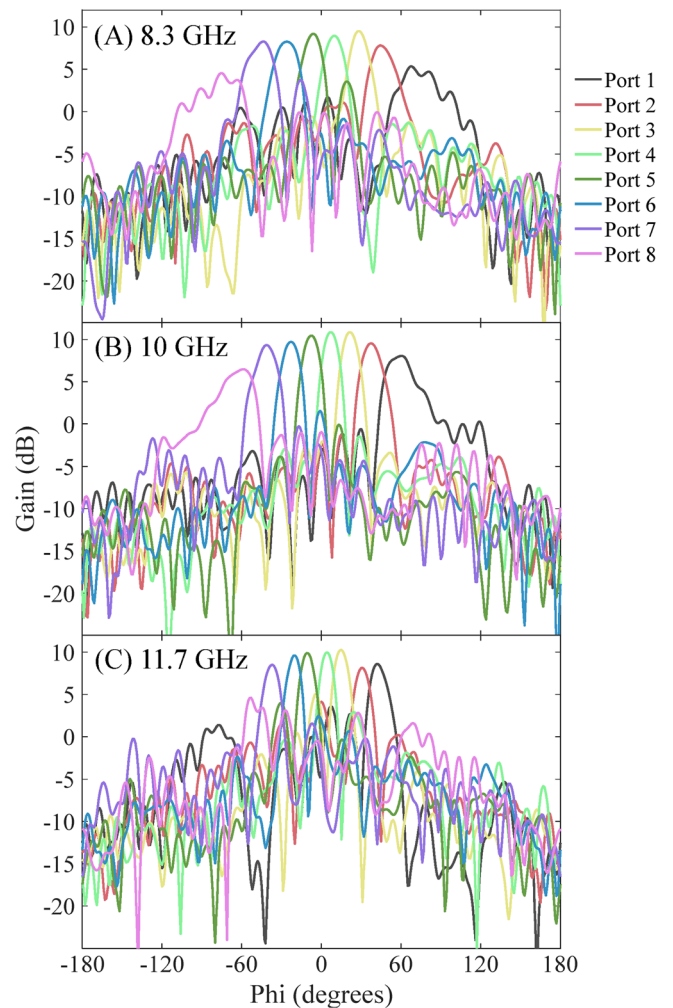re arranged in accordance with the topology BFN in Figure 1. Sections of the transmission line of the required length were used as phase shifters. The BFN has the size of 140×97 mm^2 or relative to the central wavelength of $4.7\lambda_0 \times 3.2\lambda_0$. Power is supplied by an unbalanced 50-ohm input impedance microstrip line. The distance between adjacent inputs is equal to 16 mm, which is enough for attaching coaxial connectors. The minimum distance between adjacent microstrip lines is three strip widths.

Figure 6A shows the simulation results of the reflection coefficients at all inputs (#1–#8) of the designed BFN. Analysis of the results shows that the reflection coefficients are below -15 dB in the operating range of 8.3–11.7 GHz. Figure 6B shows that transmission coefficients from input #1 to outputs #9–#16 lead in the range from -11.5 to -13.2 dB in the frequency range of 8.3–11.7 GHz. The behavior of *S*-parameters is smooth without any peaks in the operating range. Figure 5C

TABLE 2 Comparisons with other previous 8×8 multibeam antenna arrays

References	f_0 (GHz)	Bandwidth (%)	Size (λ^2)	Amplitude imbalance (dB)	Phase imbalance (deg.)	Scan angle (deg.)
19	60	16.6	$0.19\lambda_0 \times 0.29\lambda_0$[a]	±2.5	±22	±60
20	29.5	10.2	$13.5\lambda_0 \times 6\lambda_0$	±2	±15	±55
21	28	18	$3.9\lambda_0 \times 5.7\lambda_0$	±2.2	N/A	±61
22	1.9	10.5	$3.8\lambda_0 \times 2.9\lambda_0$	±1.5	±12	±55
23	2.4	5.5	$1.9\lambda_0 \times 1.4\lambda_0$[a]	±1.9	±12	±54
24	60	16.4	$12\lambda_0 \times 16\lambda_0$	N/A	N/A	±56
25	3	33	$1.7\lambda_0 \times 1.5\lambda_0$[a]	±0.5	±10	±54
26	60	9.6	$5.1\lambda_0 \times 6.5\lambda_0$	N/A	±29	±40
27	2.4	5.5	$3.3\lambda_0 \times 4.7\lambda_0$[a]	±1.9	±12	±60
This work	10	34	$4.7\lambda_0 \times 4\lambda_0$	±2.5	±20	±60

Note: The bandwidth is calculated as $2\left(f_p - f_r\right)/\left(f_p + f_r\right)$, where f_p and f_r is the upper and lower boundaries of the frequency range at the level of the amplitude ≤ -10 dB. N/A represents "not applicable," which means the value is not found in the reference.
[a]Represents the size of BFN without an antenna array.

demonstrates the isolations of input port #1 which are better than -20 dB within the operational bandwidth. The phase distribution at the outputs of the proposed BFN has the following form

antenna has an ultra-wideband slotted traveling wave radiator based on a slot with a smoothly varying profile.[40] The ultra-wideband properties of the Vivaldi antenna are provided due to a smooth transformation of the charac-

$$\varphi_{m,n} = \begin{bmatrix} 199.5° & 207° & 216.8° & 267° & 113.8° & 126.8° & 131.7° & 180.9° \\ 24.2° & 75.4° & 132.3° & 223° & 117.7° & 172.1° & 222° & 313.3° \\ 232.4° & 327.8° & 66.4° & 204.4° & 143.7° & 238.4° & 341° & 115° \\ 87.6° & 219.2° & 15.3° & 183° & 178.1° & 306.5° & 104.3° & 273.7° \\ 290.9° & 119.6° & 310.4° & 179.6° & 208.7° & 38.6° & 219° & 92.5° \\ 137.2° & 8.9° & 242.4° & 153.3° & 228.3° & 102.1° & 333.8° & 244.5° \\ 341.7° & 257.2° & 173.4° & 129.7° & 251.2° & 165.8° & 90.2° & 44.6° \\ 197.2° & 147.8° & 121.7° & 110.1° & 286° & 235.2° & 213.4° & 203.9° \end{bmatrix}. \tag{33}$$

It can be summarized from the obtained results that the designed 8×8 BFN based on the slot-line transitions and magic-Ts has the following characteristics: operating frequency range from 8.3 to 11.7 GHz; the amplitude at the outputs is -13.5 ± 2.5 dB; maximum phase imbalance is $\pm20°$; the isolation of all inputs is below -22 dB, and the reflection coefficients are below -15 dB over the operating range.

3.3 | Antenna array

We connect the proposed 8×8 BFN with a linear antenna array comprising Vivaldi-type antennas. This

teristic impedance of the slot line to ensure the effective radiation of the slot segments with dimensions on the order of half a wavelength. For this kind of antenna, the radiation is carried out along the PCB that leads to a definite advantage over other antennas. The topology of the antenna array is shown in Figure 5. The dimensions of the module were 140×120 mm^2 ($4.7\lambda_0 \times 4\lambda_0$). The distance between the radiators of the antenna array is 15 mm. To improve the impedance matching of the extreme radiators, the copper conductor at the edges of the array is extended by a quarter of the average wavelength.

Preliminary, we calculated the characteristics of an eight-element antenna array based on used Vivaldi

antennas. The voltage standing wave ratio (VSWR) at the inputs is equal to 1.75 in the operating range. The beam width of lobes exceeds 110° in the *H*-plane and no more than 13° in the *E*-plane. The radiation in the opposite direction does not exceed the level of −15 dB. As a result, we obtain the eight-beam antenna array in the 120° sector by combining the proposed BFN with the antenna array into a single structure.

Figure 7 shows the *S*-parameters of the uniform structure (BFN and Vivaldi antenna array) in the X-band. Reflection coefficients from all ports #1–#8 are below the level of −15 dB as shown in Figure 7A. The isolation level is below −20 dB in the operating range (Figure 7B,C).

The aperture of the antenna array forms a beam at a certain angle with its own directional pattern when a signal is applied to one of the 8 inputs. Figure 8 shows the azimuthal angle dependence of the gain at the central frequency 10 GHz and boundary frequencies of 8.3 GHz and 11.7 GHz, respectively. The gain peak reaches 12 dB and the sidelobe level of the beams does not exceed 9 dB. The average half-power beam widths vary from 13° to 25° in the azimuth plane and 107° to 113° in the elevation plane while the beam scan range is from −61° to 59° in the azimuth plane.

Finally, the synthesized BFN with antenna array is compared to several previously described designs early which exhibit broadband wide-angle scanning characteristics. Table 2 presents the comparative results of only 8×8 BFN with/without multibeam antenna arrays in the characteristics of central frequency (f_0), bandwidth, dimension, amplitude and phase imbalance, and scan angle. The proposed design has the superiorities of bandwidths, good isolation, compact size, and very simple design in comparison with other 8×8 BFN and multibeam antenna arrays. We believe that the proposed eight-channel multi-beam antenna array can be easily fabricated using PCB technology and can compete with known systems based on the Butler matrix.

4 | CONCLUSION

In this work, we synthesized a novel 8×8 BFN for multibeam antenna array applications. The proposed BFN has 6 less path crossings than the classic Butler matrix when the inputs and outputs are sequentially numbered. The BFN topology was proposed in the form of a three-layer PCB with dimensions $4.67\lambda_0 \times 4\lambda_0$ mm using broadband slot-line transition and magic-Ts in the X-band. The analysis of the frequency-dependent characteristics of the BFN was carried out by numerical simulation. The BFN was demonstrated a good performance in the operating frequency range from 8.3 to 11.7 GHz. The amplitude at outputs #9–#16 corresponds to -13.5 ± 2.5 dB. The isolation of all inputs was below −22 dB, and the reflection coefficients were at the level of −15 dB over the entire operating range. Moreover, we presented an eight-channel antenna array based on the synthesized BFN and Vivaldi antennas, which forms a multibeam mode of operation. The eight beams cover a spatial range of 120° with a peak gain of 12 dB. The obtained results validate that the proposed broadband and wide-angle multibeam antenna array based on the novel synthesized topology of BFN can be a good candidate for radar and satellite communication.

DATA AVAILABILITY STATEMENT

The data that support the findings of this study are available from the corresponding author upon reasonable request.

ORCID

Ihar Faniayeu https://orcid.org/0000-0002-2411-9044

REFERENCES

1. Shelton J, Kelleher KS. Multiple beams from linear arrays. *IRE Trans Antennas Propag.* 1961;9(2):154-161.
2. Delaney WP. An RF multiple beam-forming technique. *IRE Trans Military Electron.* 1962;6(2):179-186.
3. Denidni TA, Libar TE. Wide band four-port Butler matrix for switched multibeam antenna arrays. *Beijing, China: 14th IEEE Proc on Personal, Indoor and Mobile Radio Commun (PIMRC).* Vol 3; IEEE; 2003:2461-2464.
4. Ross G, Schwartzman L. Continuous beam steering and null tracking with a fixed multiple-beam antenna array system. *IEEE Trans Antennas Propag.* 1964;12(5):541-551.
5. Sorbello RM, Karmel PR, Gruner RW. Feed array and beam forming network design for a reconfigurable satellite antenna. *Quebec, Canada: 1980 Antennas and Propag Society Int Symp.* Vol 18; IEEE; 1980:1625457.
6. Rashid-Farrokhi F, Tassiulas L, Liu KJR. Joint optimal power control and beamforming in wireless networks using antenna arrays. *IEEE Trans on Commun.* 1998;46(10):1313-1324.
7. Nolen J. *Synthesis of Multiple Beam Networks for Arbitrary Illuminations.* Johns Hopkins Univ; 1965.
8. Blass J. Multidirectional antenna, a new approach to stacked beams. *IRE Int Conf Rec.* 1960;8:48-50.
9. Rotman W, Turner RF. Wide-angle microwave lens for line source applications. *IEEE Trans Antennas Propag.* 1963;11(6):623-632.
10. Butler J, Lowe R. Beam-forming matrix simplifies design of electronically scanned antennas. *Electron Des.* 1961;9:170-173.
11. Kwang TKG, Gardner P. 4×4 Butler matrix beam forming network using novel reduced size branchline coupler. *31st Eur Microw Conf;* IEEE; 2001:1-4.
12. Wincza K, Gruszczynski S, Sachse K. Reduced sidelobe four-beam antenna array fed by modified Butler matrix. *Electron Lett.* 2006;42(9):508-509.

13. Wincza K, Gruszczynski S, Sachse K. Broadband planar fully integrated 8×8 Butler matrix using coupled-line directional couplers. *IEEE Trans Microw Theory Tech*. 2011;59(10): 2441-2446.

14. Crestvolant VT, Iglesias PM, Lancaster MJ. Advanced Butler matrices with integrated bandpass filter functions. *IEEE Trans Microw Theory Tech*. 2014;62(11):2659-2672.

15. Karavassilis N, Davies DEN, Guy CG. Experimental HF circular array with direction finding and null steering capabilities. *Proc Inst Elect Eng—Microw Antennas Propag*. 1986;133(2): 147-154.

16. Angelucci A, Audagnotto P, Corda P, Piovano B. Multiport power amplifiers for mobile-radio systems using microstrip Butler matrices. *Int Symp Antennas Propag*. 1994;1:628-631.

17. Staszek K, Gruszczynski S, Wincza K. Broadband measurements of S-parameters utilizing 4×4 Butler matrices. *IEEE Trans Microw Theory Tech*. 2013;61(4):1692-1699.

18. De Lillo RA. A high performance 8-input, 8-output Butler matrix beamforming network for ultra-broadband applications. *IEEE Antennas Propag Int Symp Dig*. 1993;1:474-477.

19. Chin T-Y, Wu J-C, Chang S-F, Chang C-C. A V-band 8×8 CMOS Butler matrix MMIC. *IEEE Trans Microw Theory Tech*. 2010;58(12):3538-3546.

20. Zhong L-H, Ban Y-L, Lian J-W, et al. Miniaturized SIW multibeam antenna array fed by dual-layer 8×8 Butler matrix. *IEEE Antennas Wireless Propag Lett*. 2017;16:3018-3021.

21. Wang X, Laabs M, Plettemeier D, et al. 28 GHz Multi-beam antenna array based on a compact wideband 8×8 Butler matrix. *Int Symp on Antennas and Propag & USNC/URSI National Radio Science Meeting*. IEEE; 2018:2177-2178.

22. Adamidis GA, Vardiambasis IO, Ioannidou MP, Kapetanakis TN. Design and implementation of single-layer 4×4 and 8×8 Butler matrices for multibeam antenna arrays. *Int J Antennas Propag*. 2019;12:1645281.

23. Shao Q, Chen F-C, Wang Y, Chu Q-X. Design of 4×4 and 8×8 filtering Butler matrices utilizing combined 90° and 180° couplers. *IEEE Trans Microw Theory Tech*. 2021;69(8):3842-3852.

24. Li Y, Luk K-M. A multibeam end-fire magnetoelectric dipole antenna array for millimeter-wave applications. *IEEE Trans Antennas Propag*. 2016;64(7):2894-2904.

25. Wincza K, Gruszczynski S. Broadband integrated 8×8 Butler matrix utilizing quadrature couplers and Schiffman phase shifters for multibeam antennas with broadside beam. *IEEE Trans Microw Theory Tech*. 2016;64(8):2596-2604.

26. Park Y, Bang J, Choi J. Dual-circularly polarized 60 GHZ beam-steerable antenna array with 8× 8 butler matrix. *Appl Sci*. 2020;10(7):2413.

27. Kaminski P, Wincza K, Gruszczynski S. Switched-beam antenna array with broadside beam fed by modified Butler matrix for radar receiver application. *Microw Opt Technol Lett*. 2014;56(3):732-735.

28. Sodin LG. Method of synthesizing a beam-forming device for the N-beam and N-element array antenna, for any N. *IEEE Trans Antennas Propag*. 2012;60(4):1771-1776.

29. Sun L, Zhang G, Sun B. Method of synthesizing orthogonal beam-forming networks using QR decomposition. *IEEE Access*. 2018;7:325-331.

30. Sazonov DM, Gridin AN, Mishustin BA. *Microwave Circuits*. Mir; 1982.

31. Knorr JB. Slotline transitions. *IEEE Trans Microw Theory Tech*. 1974;22:548-554.

32. Soltysiak P, Chramiec J. Design of broadband from microstrip to slotline. *Electron Lett*. 1994;30(4):328-329.

33. Schuppert B. Microstrip/slotline transitions: modeling and experimental investigation. *IEEE Trans Microw Theory Tech*. 1988;36(8):1272-1282.

34. Zinieris MM, Sloan R, Davis LE. A broadband microstrip to slot-line transition. *Microw Opt Technol Lett*. 1998;18(5): 339-342.

35. Masayoshi A, Ogawa H. A new MIC magic-T using coupled slot lines. *IEEE Trans Microw Theory Tech*. 1980;28(6):523-528.

36. Kongpop U, Wollack EJ, Papapolymerou J, Laskar J. A broadband planar magic-T using microstrip-slotline transitions. *IEEE Trans Microw Theory Tech*. 2008;56(1):172-177.

37. Feng W. Compact planar magic-T based on the double-sided parallel-strip line and the slotline coupling. *IEEE Trans Microw Theory Tech*. 2010;58(11):2915-2923.

38. Howe H. *Stripline Circuit Design*. Artech House; 1974.

39. Marynowski W, Mazur J. Investigation of multilayer magic-T configurations using novel microstrip-slotline transitions. *PIER*. 2012;129:91-108.

40. Wang P, Zhang H, Wen G, Sun Y. Design of modified 6-18 GHz balanced antipodal Vivaldi antenna. *PIER C*. 2012;25: 271-285.